Understanding pH-Dependent Selectivity of Alamethicin K18 Channels by Computer Simulation

D. Peter Tieleman,* Vitali Borisenko,† Mark S. P. Sansom,‡ and G. Andrew Woolley†

*Department of Biological Sciences, University of Calgary, Calgary, Alberta T2N 1N4, Canada; †Department of Chemistry, University of Toronto, Toronto, Ontario M5S 3H6, Canada; and ‡Laboratory of Molecular Biophysics, Department of Biochemistry, University of Oxford, Oxford OX1 3QU, United Kingdom

ABSTRACT Alamethicin K18 is a covalently linked alamethicin dimer in which the glutamine residue at position 18 in each helix has been replaced by a lysine residue. As described in previous work, channels formed by this peptide show pH-dependent selectivity. The maximum anion selectivity of the putative octameric conducting state is obtained at pH 7 or lower. Inasmuch as no change in selectivity is seen between pH 7 and pH 3, and because protons are expected to be in equilibrium with the open state of the channel during a selectivity measurement, the channel is believed to be fully charged (i.e., all eight lysines protonated) at pH 7. In an effort to understand how such a highly charged channel structure is stable in membranes and why it is not more selective for anions, we have performed a number of computer simulations of the system. Molecular dynamics simulations of 10 ns each of the octameric bundle in a lipid bilayer environment are presented, with either zero, four, or eight lysines charged in the absence of salt, and with eight lysines charged in the presence of 0.5 M and 1 M KCl. When no salt is present and all lysines are charged, on average 1.9 Cl^- ions are inside the channel and the channel significantly deforms. With 0.5 M KCl present, 2.9 Cl^- ions are inside the channel. With 1 M KCl present, four Cl^- ions are present and the channel maintains a regular structure. Poisson-Boltzmann calculations on models of the octameric channel also predict an average of 2–4 Cl^- ions near the lysine residues as a function of ionic strength. These counterions lower the apparent charge of the channel, which may underlie the decrease in selectivity observed experimentally with increasing salt concentrations. We suggest that to increase the selectivity of Alm K18 channels, positive charges could be engineered in a narrower part of the channel.

INTRODUCTION

A key feature of ion channels is their ability to select among different ions while maintaining high ion throughput. Crystal structures of highly selective chloride and potassium channels have shown that these channels provide an environment, in the form of a selectivity filter, that is exquisitely tailored to the type of ion they conduct (Doyle et al., 1998; Dutzler et al., 2002). In many other, typically less selective, channels, selectivity is achieved by other means. Such channels include porins (Phale et al., 2001; Zeth et al., 2000), peptide channels (Sansom, 1991), mechanosensitive channels (Chang et al., 1998), and ligand-gated channels (Adcock et al., 1998). In a previous study on alamethicin variants, Starostin et al. (1999) made mutations in the antimicrobial peptide alamethicin that converted channels formed by this peptide from mildly cation selective to mildly anion selective. This change in selectivity was achieved by mutating pore-lining glutamine residues to lysines. Interestingly, this resulted in a pH-dependent selectivity (Borisenko et al., 2000). At high pH, where the lysines are all thought to be uncharged, the channel has the same selectivity as the wild-type alamethicin with glutamines. At intermediate pH values, the selectivity decreases, and at a pH of 7 and below, the channel is anion selective. Inasmuch as no change in selectivity was seen between pH 7 and pH 3, and because protons are expected to be in equilibrium with the open state of the channel during a selectivity measurement, the channel is believed to be fully charged (i.e., all eight lysines are protonated) at pH 7.

At first glance, such a highly charged aggregate might not be expected to be stable in the relatively low dielectric membrane environment. In addition, if it were stable, one might intuitively have expected such a structure to have higher anion selectivity than that measured experimentally ($P_{Cl^-}/P_{K^+} = 4$) (Borisenko et al., 2000). In an attempt to calculate the ion selectivity to be expected for a fully charged octameric Alm K18 channel, Borisenko et al. (2000) used the Nernst-Planck equation and electrostatic potential profiles obtained from numerically solving the linearized PB equation for channel models. As has been stated previously, this approach is overly simplistic (Kuyucak et al., 2001; Roux, 2002) and, although it may capture certain aspects of channel permeation under a limited set of conditions (Woolley et al., 1997), we show that it is not applicable to the present case.

In this paper we use extended MD simulations as well as PB calculations to investigate the properties of models of Alm K18 octameric channels in lipid membranes. Effects of different protonation states of the lysines and of different salt concentrations on the channel structure and the charge distribution inside the channel lead us to the conclusion that Cl^- counterions loosely associated with the ring of lysine residues may play a major role in stabilizing the channel. In

Submitted March 20, 2002, and accepted for publication October 8, 2002.

Address reprint requests to Peter Tieleman, Fax: 403-289-9311; E-mail: tieleman@ucalgary.ca; or Andrew Woolley, Fax: 416-978-0675; E-mail: awoolley@chem.utoronto.ca.

Abbreviations used: PB, Poisson-Boltzmann; MD, molecular dynamics; RMSD, root mean-square deviation.

0006-3495/03/03/1464/06 $2.00

addition, these counterions presumably play a primary role in determining the anion selectivity of the system.

METHODS

MD simulations

The construction of molecular models of the Alm K18 octameric channel has been described before by Borisenko et al. (2000). Alm K18 is a dimer, consisting of two alamethicin peptides in which Gln-18 has been replaced by Lys, which are covalently tethered together (You et al., 1996). A charge state of +4 was created by deprotonating the first lysine of each dimeric Alm K18. A charge state of 0 was created by deprotonating all lysine residues. Starting structures for MD simulations were created as described before for other alamethicin channels (Tieleman et al., 2002). The starting model of the helix bundle and an overview snapshot of the whole system are given in Fig. 1. The force field used and most of the simulation parameters were also the same as in Tieleman et al. (2002), except as specified below. A 1.0-nm cutoff for Lennard-Jones and short-range Coulomb interactions was used, combined with particle-particle-particle-mesh (Hockney and Eastwood, 1988; Berendsen et al., 1995) for long-range Coulomb interactions in the position restraint simulations and the first 3 ns of K18-plus4 and K18-plus8. Because the use of particle-particle-particle-mesh causes technical difficulties with pressure scaling, simulations were run under constant volume conditions. Particle mesh Ewald was used in the remainder of the simulations with a short-range Coulomb cutoff of 0.85 nm, with constant volume to be consistent with the previous simulations (Sagui and Darden, 1999). Our more recent simulations use particle mesh Ewald with constant area or constant pressure, but the differences should be modest on the 10-ns timescale of the present simulations. In three simulations of 10-ns each, the effect of having 0 charge on the lysines (high pH), +4 charge (intermediate pH), and +8 (low pH) was studied, with only counter ions present. Two additional simulations of the +8 charge state examined the effect of the presence of salt. First, 2-ns simulations were performed with the protein nonhydrogen atoms restrained to their original positions in the model using harmonic restraints with a force constant of 1000 kJ mol^{-1} nm^{-1} to allow the added salt solution to equilibrate. These simulations were followed by 10-ns simulations without position restraints. A summary of all simulations is given in Table 1.

PB calculations

The electrostatics calculations were made using UHBD version 5.1 (Davis et al., 1991) (with some local modifications, Adcock et al. (1998)) and partial atomic charges from the Quanta/Charmm22 parameter set. The model system consisted of a low dielectric slab of thickness 40 Å, into which an Alm K18 channel structure was inserted. The slab was generated from dummy atoms on a simple cubic lattice with a 2.5-Å spacing. The boundary of the protein and low dielectric slab were defined by the solvent-accessible surface, and the dielectric constant for the protein was set at 4. Both the dielectric inside the model pore (representing solvent) and the bulk solvent dielectric were set at 78. To calculate electrostatic potential profiles for permeating ions, a trajectory through the channel was defined using the program HOLE (Smart et al., 1997). Because the channel is relatively wide and straight, this trajectory corresponded roughly to the channel's z axis. The electrostatic energy of a +1 e probe charge at successive positions along the pore trajectory was then calculated using the UHBD program for different values of the Stern radius and the ionic strength, both with the linearized and the nonlinear PB equation.

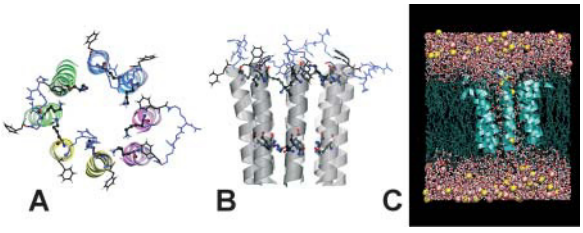

FIGURE 1 Snapshots of the initial model (*A* and *B*), and the model in the lipid bilayer environment used in the simulations (*C*). The alamethicin (Alm) variant used is a covalently linked dimer, colored by Alm molecule in *A*. The linker is attached to the C-terminus of two helices and is shown in blue. Also shown are the modified C-terminal phenylalanine residues and the critical Lys-18 residues. In *B*, in addition to these residues, Gln-7, which forms the narrowest part of the pore, is also highlighted. Panels *A* and *B* were made with MolScript (Kraulis, 1991) and Render (Merritt and Bacon, 1997); panel *C* was made with VMD (Humphrey et al., 1996).

TABLE 1 Summary of the simulations

	Position restraint	Run	System
K18-plus0	25 ps	10 ns	95 lipids, 3532 water, Alm unprotonated
K18-plus4	25 ps	10 ns	95 lipids, 3528 water, 4 Cl^-, Alm 4 Lys protonated
K18-plus8	25 ps	10 ns	95 lipids, 3524 water, 8 Cl^-, Alm 8 Lys protonated
K18-0.5 M	2 ns	10 ns	95 lipids, 3460 water, 32 K^+, 40 Cl^-, Alm 8 Lys protonated
K18-1 M	2 ns	10 ns	95 lipids, 3396 water, 64 K^+, 72 Cl^-, Alm 8 Lys protonated

Single-channel measurements

Single-channel current-voltage relationships were obtained exactly as described in Borisenko et al. (2000) using KCl gradients of 1.3 M/0.1 M; 1.3 M/0.01 M, and 0.2 M/0.01 M (pH 3.0). Selectivities were calculated from reversal potentials using Eq. 1 of Borisenko et al. (2000).

RESULTS

MD simulations

First we examined the stability of the channel structures by comparing backbone RMSD. Fig. 2 shows the RMSD of the

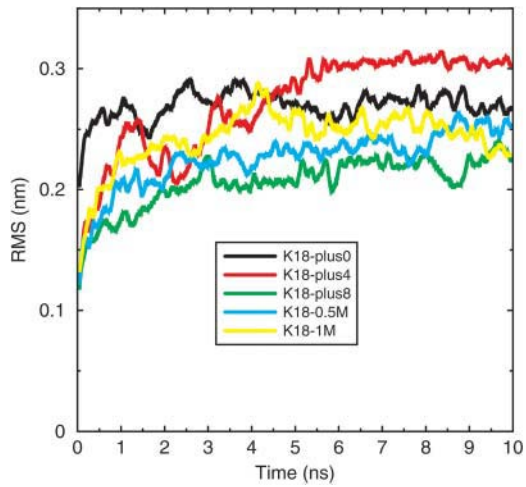

FIGURE 2 RMSD from the starting model for all five simulations, calculated for the backbone atoms only after fitting on the C_α carbons.

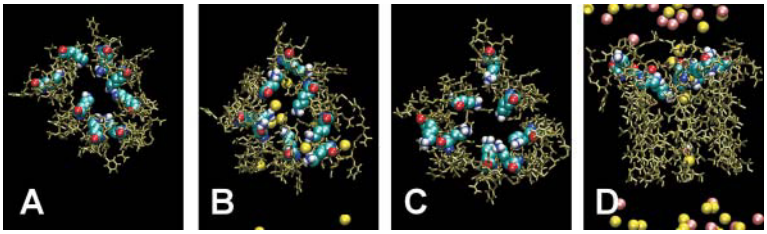

FIGURE 3 Snapshots after 10 ns for (*A*) K18-plus0, (*B*) K18-plus8, (*C*) K18-1 M, and (*D*) K18-1 M seen from the side. In all four snapshots, the Lys-18 residues are shown as space filling. Chloride ions are yellow, potassium ions pink. Note that *A* has no ions, *B* has eight chloride ions as counterions for the eight charged lysines, and *C* and *D* are the same system, with 1 M KCl in addition to counterions. Ions are present but not shown in *C*. Figures were made with VMD.

backbone, after fitting on the C_α atoms, relative to the starting structure for all five simulations. Interestingly, the lowest RMSD is found in the K18-plus8 simulation, despite the high charge density near the lysines. In all cases, the peptides remain mostly helical (details not shown). However, the structure of the bundles after 10 ns is more different than perhaps the RMSDs suggest. In Fig. 3, snapshots are shown after 10 ns of simulation of the pore and the lysine region from K18-plus0 (Fig. 3 *A*), K18-plus8 (Fig. 3 *B*), and K18-1 M (Fig. 3 *C*). In Fig. 3 *A*, the lysine side chains point toward the middle of the channel and in some cases form hydrogen bonds with one another. In Fig. 3 *B*, some of the lysine side chains point almost out of the channel, minimizing the interactions between the eight charges in a relatively small volume. Also shown are the chloride ions. The channel has deformed compared to its initial, almost symmetrical structure. In Fig. 3 *C*, the channel is more regular, and despite the high charge density, all but one of the side chains still point at the center of the channel. Ions are not shown in Fig. 3 *C* as they would obscure the Lys residues, but Fig. 3 *D* shows the same system at the same time from the side with the ions included.

Fig. 4 shows the average charge distribution in the channel, calculated by dividing the channel into 100 slices along the *z* axis (the channel axis). In the force field used, the NZ atom of lysine has a charge of $-0.83\ e$ in the neutral version of lysine (with $+0.415$ for HZ1 and HZ2), and a charge of $0.129\ e$ for the protonated version (with $+0.248$ for HZ1, HZ2, and HZ3). Thus, in the case of K18-plus0, the NZ graph mainly shows where the NZ atoms are located with respect to the ions, but the average charge density due to the lysine side chains is zero. The graphs of K18-plus8 show the total charge density due to the lysine side chains, counting NZ as having a $+1\ e$ charge. In both K18-plus8 and K18-1 M graphs, the lysines form two separate distributions, roughly separated by 1 nm. When integrating the charge density over 3–5 nm, the total charge of NZ (including the attached hydrogens) in K18-plus8 and K18-1 M is 8 *e*, as expected. The total chloride charge inside the channel between 3 and 5 nm is $-4\ e$ in K18-1 M, $-2.9\ e$ for K18-0.5 M, and $-2.1\ e$ for K18-plus8. Note that after integration of Fig. 4, the results must be multiplied by the *x,y* area (the plane parallel to the membrane interface, with an area of 34.4 nm^2) of the system to get absolute charges.

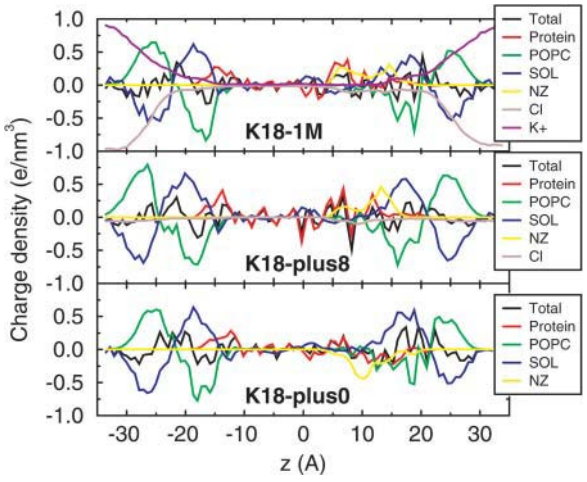

FIGURE 4 Charge density along an axis parallel to the channel pore for K18-plus0, K18-plus8, and K18-1 M. NZ refers to the NZ atom in the lysine side chain. In K18-1 M and K18-plus8, the charge of the attached hydrogens has been summed into the NZ atom, so that its charge is +1. In K18-plus0, the total charge of NZ plus its two attached hydrogens is 0.

In all cases, ions are quite mobile on the 10-ns timescale of the simulations. Even when only counterions are present they interact with the channel. Fig. 5 shows the trajectories of the ions in each of the simulations in the *z* direction. The ions exchange rapidly between bulk and channel, especially at higher salt concentrations.

PB calculations

Using the same set of channel models generated in previous work (Borisenko et al., 2000), we performed a new set of PB calculations to systematically test the effect of the choice of Stern exclusion radius and the difference between the linearized and the nonlinear PB equation. The electrostatic potentials were calculated along a trajectory through the pore as calculated using the program HOLE (Smart et al., 1997). The pore radius profiles are shown in Fig. 6 for five different K18 models. The electrostatic potentials, averaged over all five structures, are shown in Fig. 7 for three different values of the ionic strength and the Stern exclusion radius, for both the linearized and nonlinear PB equation. Clearly, there is a large difference between the results from the linear and nonlinear PB equation. The linearized version predicts a much higher barrier than the nonlinear PB equation. Near the ring of lysine residues the local potential becomes much greater than kT so that average ion-ion distances become

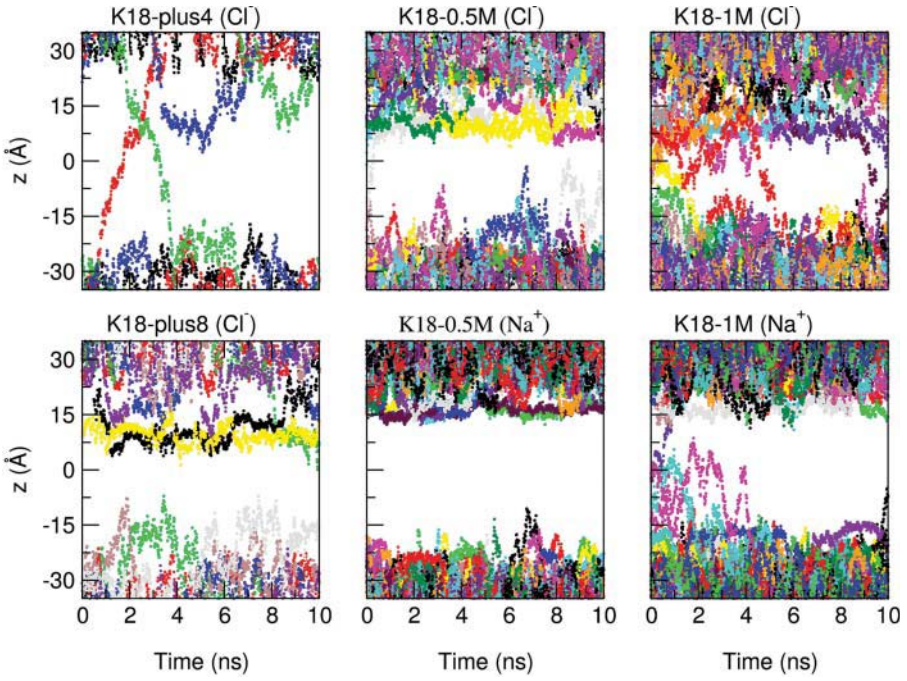

FIGURE 5 Ion trajectories in the z dimension during 10-ns simulations. The middle of the channel/bilayer is at $z = 0$ Å. Points in the trajectory are separated by 10 ps.

small and the linearized form of the PB equation is not applicable (Berry et al., 2000). In Fig. 8 the integrated number of chloride ions in the channels, obtained from the Boltzmann factor at the calculated potentials, is shown. The Lys-18 residues are found at a z coordinate of ~10–14 Å. The total number of chlorides in the channel depends on the Stern exclusion radius used, although the difference between 1 and 2 Å is not very large. A radius of 3 Å approaches the channel radius and has a large effect. The total number of chlorides in the channel increases with increasing ion strength. At 1 M, the total number is ~4.3–4.6, depending on Stern radius of 1 or 2 Å at $z = 15$ Å, at 100 mM the total number is 2.5–3.2, and at 10 mM 2.0–2.6 ions. The numbers become unrealistically high for a Stern radius of 3 Å (~10, 12, and 15 respectively for 10 mM, 100 mM, and 1 M). Because the calculated potentials are much higher in the case of the linear PB equation, the resulting ion numbers are completely unrealistic.

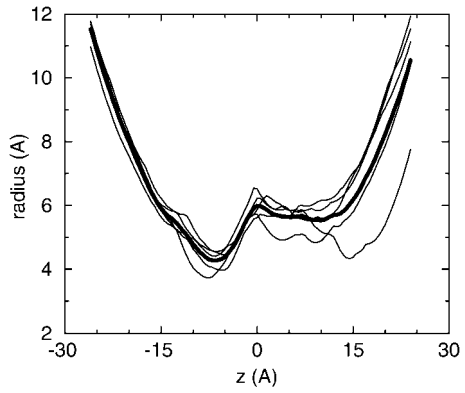

FIGURE 6 Pore radius profile of the five models used for the PB calculations (*thin lines*) plus their average radius profile, calculated with HOLE (Smart et al., 1997).

Single-channel measurements

Previous experimental measurements of cation versus anion selectivity were extended to include measurements of reversal potentials at lower ionic strengths. The (P_{Cl^-}/P_{K^+}) selectivity calculated from these data are collected in Table 2. As overall ionic strength increases, selectivity is observed to decrease.

DISCUSSION

The central results of the present simulations are that fully charged K18 channels appear to be stable in membranes and that significant counterion binding to Lys-18 residues occurs depending on the charge state of the channel and the salt concentration. In particular, the effective charge in the channel is greatly reduced, by 4 e, due to the permanent presence of four Cl^- ions near the eight charged lysines in K18-1 M. This feature stabilizes the channels as observed by comparing the extent of channel deformation in the K18-plus8 and K18-1 M cases (Fig. 3). Although counterion binding is implicitly included in PB calculations, the radius of the channel is narrow so that this effect may not be reliably described (Corry et al., 2000; Moy et al., 2000). Nevertheless, use of the nonlinear PB equation leads to estimates for the number of Cl^- counterions in reasonable agreement with

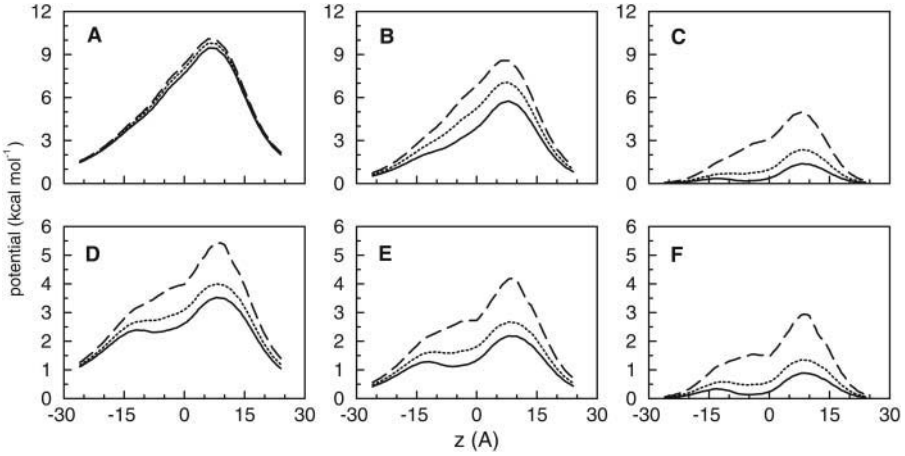

FIGURE 7 Electrostatic potential profiles calculated from the linear PB equation (*A–C*) and the nonlinear PB equation (*D–F*) for three different values of the ionic strengths and different Stern radius values (*solid line*, 1 Å; *dotted*, 2 Å; *long dashed*, 3 Å). Linear: (*A*) 10 mM; (*B*) 100 mM; (*C*) 1 M; nonlinear: (*D*) 10 mM; (*E*) 100 mM; (*F*) 1 M.

the MD simulations so long as an appropriate choice is made for the Stern radius.

The presence of counterions, the number of which varies with changes in ionic strength, is also presumably connected with the degree of anion selectivity of the channel. Experimentally, anion selectivity is observed to decrease as ionic strength increases (Table 2) consistent with a screening effect of counterions on the field created by the lysine residues

This effect helps to explain why Alm K18 channels are only mildly selective for anions over cations. Other factors may also contribute to the experimentally observed selectivity, however. For instance, we observe significant conformational changes of the lysine side chains, increasing at high charge and low salt concentration. K18-plus0 forms a regular channel and might be a reasonable model for the high pH regime. K18-1 M and K18-0.5 M might be reasonable models for pH 7 or lower, whereas K18-plus4 with salt (which we did not consider) could be a reasonable model at intermediate pH. Conformational changes of the whole channel are possible, but the overall structure of the channel except in K18-plus8 is fairly stable over 10 ns. As this timescale approaches the timescale of ion permeation, it seems less likely that major conformational changes of the channel with changes in solution pH play an important role. Also, it seems unnecessary to invoke protonation or deprotonation during permeation as a mechanism to explain the selectivity (Borisenko et al., 2000).

Of course, our supposition that such a highly positively charged channel should be highly anion selective may simply be flawed. Selectivity estimates based on the simple use of the electrostatic potential from PB calculations (linear or nonlinear) are inaccurate in this situation. Although it is not yet possible to directly link MD simulations to experimental I/V curves (Tieleman et al., 2001; Kuyucak et al., 2001), a Brownian dynamics approach for estimating selectivity (Corry et al., 2000) may be useful for this system.

Finally, we can address the key question: how can K18 or a channel of comparable complexity be made more anion selective? All our models of alamethicin channels, including Alm K18, contain a narrow part near the Gln-7 side chain (Fig. 1 *B*). It will be interesting to attempt to incorporate

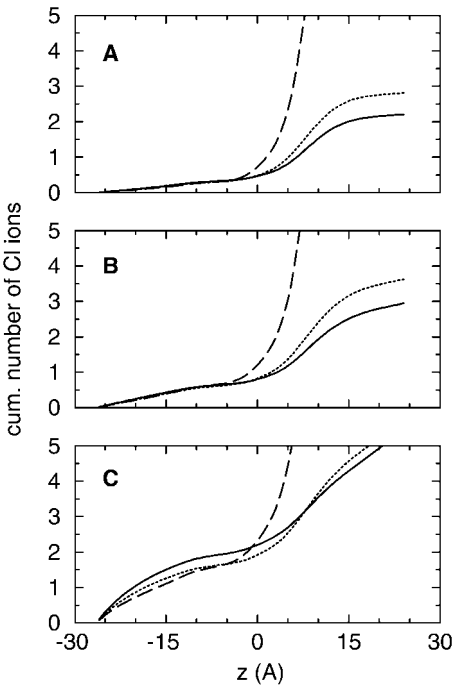

FIGURE 8 Number of chloride ions in the channel calculated from the nonlinear PB equation for different ion strengths. (*A*) 10 mM; (*B*) 100 mM; (*C*) 1 M. In each panel, solid lines are for a Stern radius of 1 Å, dotted for 2 Å, and dashed for 3 Å.

TABLE 2 Measured selectivities

Condition	Selectivity calculated from reversal potential (Cl^-/K^+)
1.3 M/0.1 M KCl gradient	2
1.3 M/0.01 M KCl gradient	4
0.2 M/0.01 M KCl gradient	8

a significant amount of positive charge in a narrow part of K18, or to introduce a modification that constricts the channel to limit counterion binding.

CONCLUSIONS

Increasing the charge density in Alm K18 only has a limited effect on selectivity because the salt distribution compensates for much of the increased charge density in the relatively wide part of the channel. The MD simulations and PB calculations predict increased counterion binding so that we expect a decreased selectivity with increasing salt concentration, which was also found experimentally. It seems that to make a highly selective anion peptide channel, it would be of interest to design a channel with a localized positive charge in a narrower part of the channel. Ultimately, a more complex architecture mimicking the chemistry of a selectivity filter from highly selective natural channels might be required.

We thank the Canadian Cystic Fibrosis Foundation and Natural Sciences and Engineering Research Council of Canada for financial support and the computing facilities at the Molecular Design and Information Technology Center (Toronto) for use of their computing facilities (G.A.W.). D.P.T. is a Scholar of the Alberta Heritage Foundation for Medical Research.

REFERENCES

Adcock, C., G. R. Smith, and M. S. P. Sansom. 1998. Electrostatics and the ion selectivity of ligand-gated channels. *Biophys. J.* 75:1211–1222.

Berendsen, H. J. C., D. van der Spoel, and R. van Drunen. 1995. GROMACS: a message-passing parallel molecular dynamics implementation. *Comp. Phys. Comm.* 95:43–56.

Berry, R. S., A. R. Rice, and J. Ross. 2000. Physical Chemistry. Oxford University Press, 2nd edition. Oxford.

Borisenko, V., M. S. P. Sansom, and G. A. Woolley. 2000. Protonation of lysine residues inverts cation/anion selectivity in a model channel. *Biophys. J.* 78:1335–1348.

Chang, G., R. H. Spencer, A. T. Lee, M. T. Barclay, and D. C. Rees. 1998. Structure of the MscL homolog from *Mycobacterium tuberculosis*: a gated mechanosensitive ion channel. *Science.* 282:2220–2226.

Corry, B., S. Kuyucak, and S. H. Chung. 2000. Tests of continuum theories as models of ion channels. II. Poisson-Nernst-Planck theory versus Brownian dynamics. *Biophys. J.* 78:2364–2381.

Davis, M. E., J. D. Madura, B. A. Luty, J. A. McCammon. 1991. Electrostatics and diffusion of molecules in solution—simulations with the University of Houston Brownian Dynamics program. *Comp. Phys. Comm.* 62:187–197.

Doyle, D. A., J. M. Cabral, R. A. Pfuetzner, A. Kuo, J. M. Gulbis, S. L. Cohen, B. T. Cahit, and R. MacKinnonl. 1998. The structure of the potassium channel: molecular basis of K^+ conduction and selectivity. *Science.* 280:69–77.

Dutzler, R., E. B. Campbell, M. Cadene, B. T. Chait, and R. MacKinnon. 2002. X-ray structure of a CLC chloride channel at 3.0 Å reveals the molecular basis of anion selectivity. *Nature.* 415:287–294.

Hockney, R. W., and J. W. Eastwood. 1988. Computer Simulation Using Particles, First Edition, Institute of Physics Publishing Ltd., New York.

Humphrey, W., A. Dalke, and K. Schulten. 1996. VMD: Visual Molecular Dynamics. *J. Mol. Graph.* 14:33–38.

Kraulis, P. J. 1991. MolScript: a program to produce both detailed and schematic plots of protein structures. *J. Appl. Crystallogr.* 24:946–950.

Kuyucak, S., O. S. Andersen, and S. H. Chung. 2001. Models of permeation in ion channels. *Rep. Prog. Phys.* 64:1427–1472.

Merritt, E. A., and D. J. Bacon. 1997. Raster3D: photorealistic molecular graphics. *Methods Enzymol.* 277:505–524.

Moy, G., B. Corry, S. Kuyucak, and S. H. Chung. 2000. Tests of continuum theories as models of ion channels. I. Poisson-Boltzmann theory versus Brownian dynamics. *Biophys. J.* 78:2349–2363.

Phale, P. S., A. Philippsen, C. Widmer, V. P. Phale, J. P. Rosenbusch, and T. Schirmer. 2001. Role of charged residues at the OmpF porin channel constriction probed by mutagenesis and simulation. *Biochemistry.* 40:6319–6325.

Roux, B. 2002. Theoretical and computational models of ion channels. *Curr. Opin. Struct. Biol.* 12:182–189.

Sagui, C., and T. A. Darden. 1999. Molecular dynamics simulations of biomolecules: long-range electrostatic effects. *Annu. Rev. Biophys. Biomol. Struct.* 28:155–179.

Sansom, M. S. P. 1991. The biophysics of peptide models of ion channels. *Prog. Biophys. Mol. Biol.* 55:139–235.

Smart, O. S., J. Breed, G. R. Smith, and M. S. P. Sansom. 1997. A novel method for structure-based prediction of ion channel conductance properties. *Biophys. J.* 72:1109–1126.

Starostin, A. V., R. Butan, V. Borisenko, D. A. James, H. Wenschuh, M. S. P. Sansom, and G. A. Woolley. 1999. An anion-selective analogue of the channel-forming peptide alamethicin. *Biochemistry.* 38:6144–6150.

Tieleman, D. P., G. R. Smith, P. C. Biggin, and M. S. P. Sansom. 2001. Simulation approaches to ion channel structure-function relationships. *Q. Rev. Biophys.* 34:473–561.

Tieleman, D. P., B. Hess, and M. S. P. Sansom. 2002. Analysis and evaluation of channel models: simulations of alamethicin. *Biophys. J.* 83:2393–2407.

Woolley, G. A., P. C. Biggin, A. Schultz, L. Lien, D. C. J. Jaikaran, J. Breed, K. Crowhurst, and M. S. P. Sansom. 1997. Intrinsic rectification of ion flux in alamethicin channels: studies with an alamethicin dimer. *Biophys. J.* 73:770–778.

You, S., S. Peng, L. Lien, J. Breed, M. S. P. Sansom, and G. A. Woolley. 1996. Engineering stabilized ion channels: covalent dimers of alamethicin. *Biochemistry.* 35:6225–6232.

Zeth, K., K. Diederichs, W. Welte, and H. Engelhardt. 2000. Crystal structure of Omp32, the anion-selective porin from *Comamonas acidovorans*, in complex with a periplasmic peptide at 2.1Å resolution. *Struct. Fold. Des.* 8:981–992.